

Fermi National Accelerator Laboratory

FERMILAB-Conf-93/384

State of Hadron Collider Physics

Paul D. Grannis

*Fermi National Accelerator Laboratory
P.O. Box 500, Batavia, Illinois 60510*

*State University of New York
Stony Brook, New York 11794*

December 1993

Presented at the *9th Topical Workshop on Proton-Antiproton Collider Physics*,
Tsukuba, Japan, October 18-22, 1993

Disclaimer

This report was prepared as an account of work sponsored by an agency of the United States Government. Neither the United States Government nor any agency thereof, nor any of their employees, makes any warranty, express or implied, or assumes any legal liability or responsibility for the accuracy, completeness, or usefulness of any information, apparatus, product, or process disclosed, or represents that its use would not infringe privately owned rights. Reference herein to any specific commercial product, process, or service by trade name, trademark, manufacturer, or otherwise, does not necessarily constitute or imply its endorsement, recommendation, or favoring by the United States Government or any agency thereof. The views and opinions of authors expressed herein do not necessarily state or reflect those of the United States Government or any agency thereof.

State of Hadron Collider Physics

Summary of the 9th \bar{p} - p Workshop, Tsukuba Japan, Oct. 18 - 22

Paul D. Grannis

State University of New York, Stony Brook NY 11794, USA

and Fermilab, P.O. Box 500, Batavia IL 60510, USA

1. Introduction

The 9th Topical Workshop on Proton-Antiproton Collider Physics in Tsukuba Japan demonstrated clearly the enormous breadth of physics accessible in hadron colliders. Although no significant chinks were reported in the armor of the Standard Model, new results presented in this meeting have expanded our knowledge of the electroweak and strong interactions and have extended the searches for non-standard phenomena significantly.

Much of the new data reported came from the CDF and DØ experiments at the Fermilab collider. Superb operation of the Tevatron during the 1992-93 Run and significant advances on the detector fronts – in particular, the emergence of the new DØ detector as a productive physics instrument in its first outing and the addition of the CDF silicon vertex detector – enabled much of this advance. It is noteworthy however that physics from the CERN collider experiments UA1 and UA4 continued to make a large impact at this meeting. In addition, very interesting summary talks were given on new results from HERA, cosmic ray experiments, on super-hadron collider physics, and on e^+e^- experiments at LEP and TRISTAN. These summaries are reported in elsewhere in this volume.

2. Strong Interaction Physics

2.1 Global Properties

Measurements of the total \bar{p} - p cross-section and the related $\rho = \text{Re}(F_{\text{nuc}})$ have been made previously at both $Spp\bar{S}$ and the Tevatron. CDF reported new σ_{tot} measurements^[1] in this conference at both $\sqrt{s} = 546$ and 1800 GeV. They employ a luminosity independent method, taking the ratio of the differential elastic rate (extrapolated to $t = 0$) and the total (elastic and inelastic) rate. Elastic and single diffractive rates are measured using 'Roman pots' embedded in the accelerator lattice, while the inelastic rates utilize the main central tracking detectors. The elastic cross-section slope, b , shown in Fig. 1 agrees well with earlier measurements at 546^[2] and 1800 GeV^[3]. The ratio $(\sigma_{el}/\sigma_{\text{tot}})$ from the new CDF data agrees well with the UA4 value at 546 GeV and is only 1.25σ above the E710 ratio at 1800 GeV, but the value of $\sigma_{\text{tot}} = 80.0 \pm 2.2$ mb extracted from these data is almost 2σ above the E710 result (72.8 ± 3.1 mb), as shown in Fig. 2. The discrepancy

presumably lies largely in the determination of the inelastic cross-section.

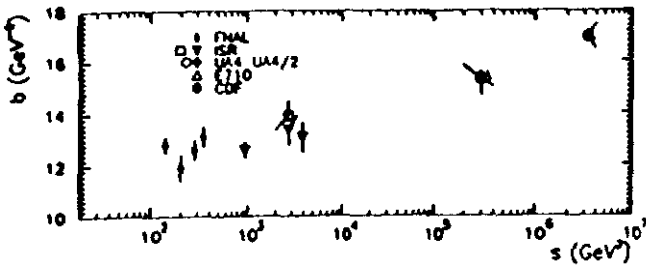


Figure 1. Elastic slope parameter b vs. s .

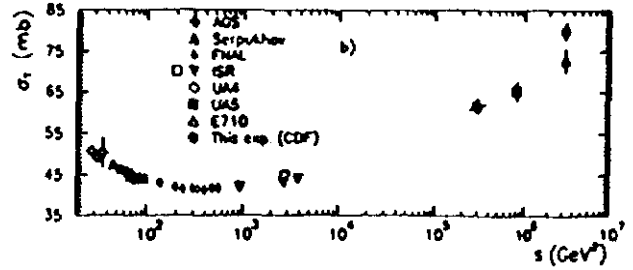


Figure 2. Total cross-section vs. s .

The old UA4 ρ value of 0.24 ± 0.04 ^[4] was over 2 standard deviations above the dispersion relation fit from lower energy data and stimulated great interest in the possibility that new physics is emerging at the TeV scale. A new measurement by the UA4/2 collaboration reported in this conference^[6] has improved statistics, beam optics and acceptance. The new result, $\rho = 0.135 \pm 0.015$ at $\sqrt{s} = 546$ GeV, shown in Fig. 3 agrees very well with the dispersion relation fits to other elastic data, and removes the need for new physics. The fit also is compared to the data on σ_{tot} in Fig. 4 and neatly splits the difference between the new CDF and older E710 result. This observation and the lack of experimental resolution of the σ_{tot} discrepancy suggests that for the present, the weighted average of the CDF and E710 total cross-section results should be used.

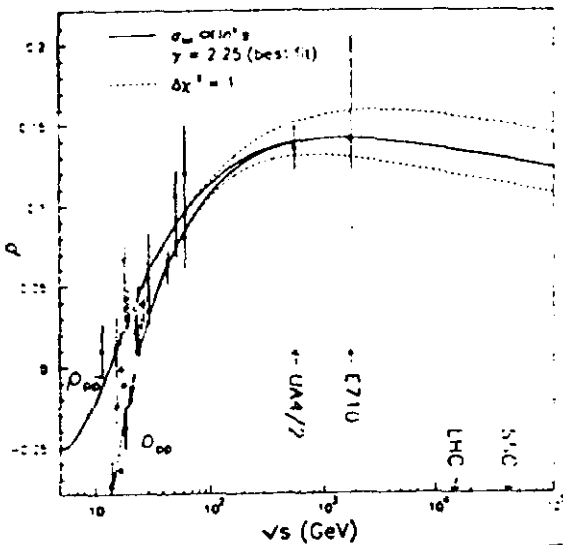


Figure 3. Real part $F_{pp}(t=0)$ vs. \sqrt{s} .

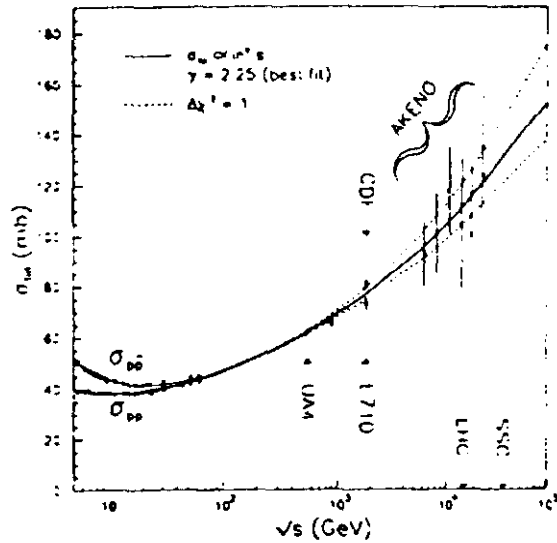


Figure 4. Predicted σ_{tot} and data vs. \sqrt{s} .

In connection with the CDF total and elastic rates measurement, the single diffractive cross-section has been determined at 546 and 1800 GeV^[6] using a single arm trigger. The cross-section $sd^2\sigma/dM^2 dt$ can be fit within the framework of a linear Pomeron trajectory $\alpha_P(t) = 1 + \epsilon + \alpha' t$, and subsidiary Regge couplings. The s and M^2 dependences both

support a supercritical Pomeron with ϵ in the range (0.1 – 0.2), consistent with the value taken from the rising total cross-section ($\epsilon = 0.112 \pm 0.013$). Evidence was sought for non-leading couplings (PP-Reggeon) and screening effects.

2.2 Inclusive Distributions

The MIMI collaboration, using UA1 data, has extended the low E_T study of inclusive production of particles at 630 GeV using a minimum bias trigger sample. Invariant inclusive cross-sections were presented for charged particles^[7] and for K_S and $\Lambda/\bar{\Lambda}$ ^[8], in the ranges $p_T < 20$ GeV/c and $|\eta| < 3$. Fits of these spectra to the form $d\sigma/dp_T^2 \sim (p_T + p_T^0)^{-n}$ are good and typically yield $n = 8.5$ and $\langle p_T \rangle$ between 0.4 and 0.6, growing with observed multiplicity. The inclusive charged particle cross-sections agree moderately well with a new QCD calculation^[9] for $p_T > 5$ GeV/c, but lie significantly above the calculation at low p_T . The K/π fractions measured from K_S or K^\pm give values around 0.08. An interesting byproduct^[8] of the Λ study is the measured equality of m_Λ and $m_{\bar{\Lambda}}$ to within 0.007%, the current best test of CPT invariance in the hyperon sector.

A defining feature of the high energy collider landscape is the observation of isolated jets of hadrons evolving from high p_T partons. The direct study of these jets permits a more direct confrontation with the underlying partonic processes and radiative corrections than the particle distributions which introduce the uncertainties associated with the jet fragmentation functions. New measurements of inclusive jet cross-sections were shown by UA1/MIMI, DØ and CDF. Using the minimum bias trigger, MIMI^[7] has extended the study of inclusive jets to $5 \leq p_T \leq 50$ GeV at 630 GeV and has shown a smooth continuation from the higher p_T UA1 data. Figure 5 shows the new and old data together, in good agreement with the QCD calculation.

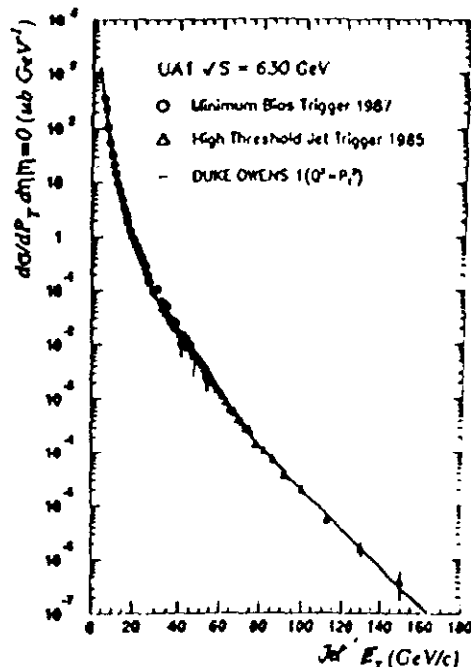


Figure 5. Jet inclusive cross-section vs. Jet E_T .

The CDF inclusive jet cross-sections have been updated with data from the recent run. For $|\eta| < 0.7$ these results^[10] agree well with the earlier CDF data and with NLO QCD^[11] out to $p_T=450$ GeV as seen in Fig. 6. CDF has returned to the question of the deviation from simple $x_T = 2E_T/\sqrt{s}$ scaling of the invariant jet cross-section, $E_T^4 E_d^3 \sigma/dp^3$. The ratio of this quantity between 546 and 1800 GeV, expected in NLO QCD to be almost 2 and only weakly dependent on x_T , is seen experimentally to rise from about 1.3 to 1.7^[10]

for the z_T range from 0.10 to 0.27. The discrepancy is over 2σ at low z_T and persists for a range of parton distribution functions and choice of scale; it illustrates the current level of precision in understanding of the QCD processes at small- x .

New jet cross-sections from $D\bar{O}$ were presented^[12] for three η regions: $|\eta| < 0.9$; $1 < |\eta| < 2$; and $2 < |\eta| < 3$. At small η these data agree within systematic errors with the NLO calculation^[11] used by CDF, and thus with the CDF data. The new feature of these data is the extension to large η ; as shown in Fig. 7 the QCD prediction continues to represent the data well, even for forward-produced jets at E_T up to 200 GeV.

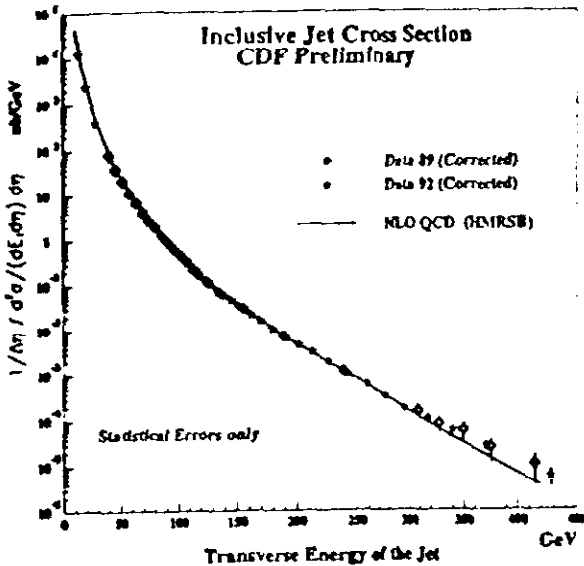


Figure 6. CDF inclusive jet cross-section at small η .

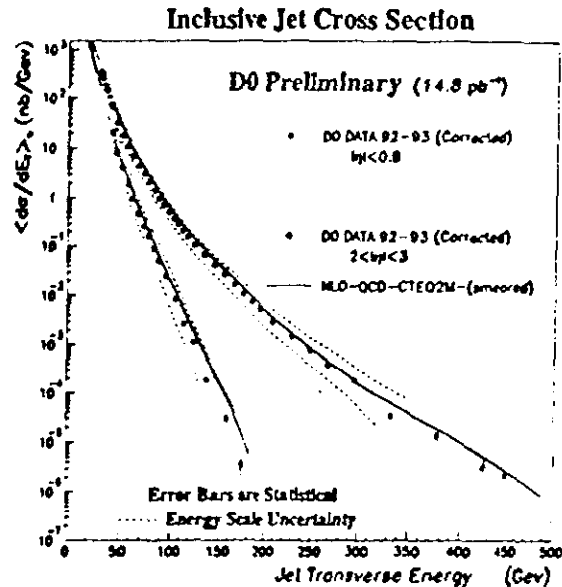


Figure 7. $D\bar{O}$ inclusive jet cross-section at small and large η .

2.3 Jet Properties

Jets are extended structures, owing to the presence of higher order gluon radiative effects at the fundamental level, as well as to fragmentation and the intrinsic spreading of hadronic showers in a real detector. Study of the energy distributions within jets can illuminate the fundamental character of partonic processes and may help distinguish the type of primary parton which initiates the jet.

$D\bar{O}$ has investigated the energy flow within jet cones in two ways. Complementing an earlier CDF study^[13], they presented^[12] the ratio of the inclusive $\eta \approx 0$ jet cross-section ratio for jets of cone size R to those with $R=0.7$. This ratio is sensitive to the high order effects of gluon emission from the parent parton and thus is a sensitive test of NLO QCD. The data of Fig. 8 show agreement between $D\bar{O}$ and CDF. The NLO QCD prediction would suggest somewhat less dependence of the cross-section on cone size for usual choices of the scale parameter, suggesting that even higher order QCD effects are at play.

An alternate approach to the same issue was presented in this meeting by $D\bar{O}$ ^[14]; they measured the fraction of the energy within a full cone of $R=1$ that is contained

within a concentric subcone of size \mathcal{R}' . This fraction measures the energy flow within a jet, and is thus sensitive to details of the underlying radiative processes. The data shown in Fig. 9 indicate a somewhat broader jet than expected from the shower Monte Carlo HERWIG, but narrower than parton-level jets.^[15] The jets show a narrowing trend as the E_T increases. Central and forward ($\eta = 2.7$) jets have the same profile up to $E_T \approx 100$ GeV; above this value, the forward jets are broader.

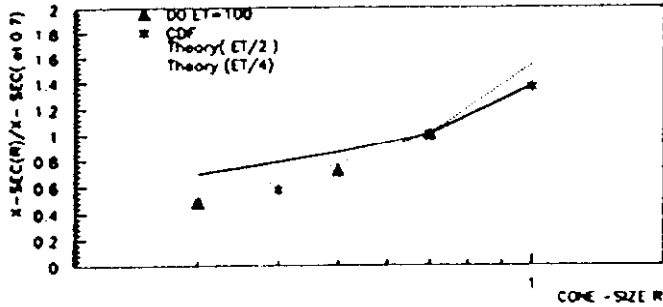


Figure 8. Jet Cone Cross-Section Ratio relative to $\mathcal{R}=0.7$.

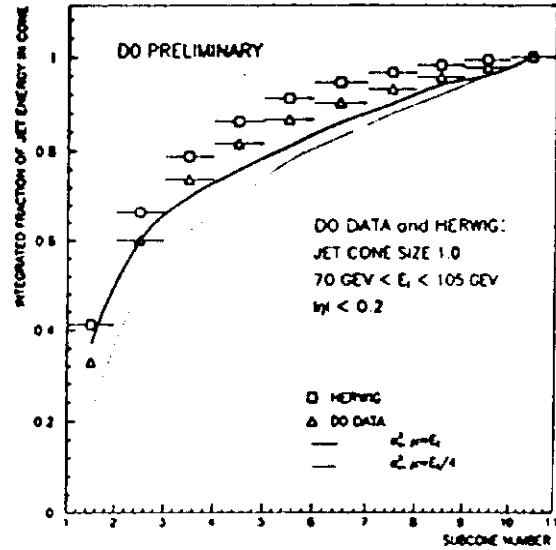


Figure 9. Integrated energy fraction in a jet subcone.

Discrimination of quark and gluon jets on an individual basis would allow interesting new QCD studies, as well as open new possibilities for heavy quark tagging and searches for heavy particles. CDF reported an analysis of quark/gluon separation^[16] using a set of moments of k_T and k_L for the particles within a jet, the jet multiplicity and EM fraction. A likelihood function was constructed from these quantities based upon the properties of HERWIG or PYTHIA Monte Carlo quark or gluon data sets. The overall likelihood function was compared to data and Monte Carlo samples of QCD di-jets, γ +jets, and W +jets, for which the quark/gluon content is expected to be quite different. Figure 10 shows the global likelihood distributions for data and Monte Carlo di-jets and γ +jets.

The quarks and gluons are moderately well distinguished and the gluon fractions extracted ($\sim 80\%$ for di-jets and $\sim 50\%$ for γ +jets) agree with expected values. This analysis is a good start on 'parton identification' schemes which should be expanded to include additional variables and correlations. The payoff here could be great.

2.4 Jet Topological Distributions

Study of the angular distributions in di-jet samples and multi-jet topological parameters are expected to permit more refined tests of the underlying QCD theory than inclusive

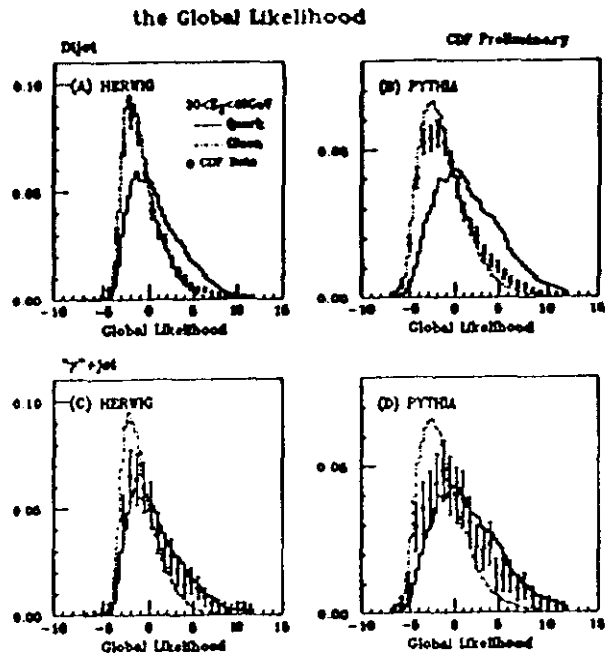


Figure 10. Global likelihood distributions for di-jet samples and $\gamma + \text{jets}$ for data, HERWIG and PYTHIA.

studies, and in many cases should give useful new information on parton distribution distributions. In these more exclusive studies, careful selection of the final states can be used to isolate particular subprocesses or regions of sensitivity to model parameters. The cm frame angular distribution of jets in di-jet events, initiated by UA2 and UA1 and continued by CDF, is a simple example of these studies. To lowest order, the angular distribution resembles the Rutherford cross-section for spin 1 exchange, but there are modifications due to QCD corrections. DØ has extended this study^[14], showing the normalized distributions $(1/N)(dN/d\chi)$, where χ is $e^{2\eta^*}$ (η^* is the jet rapidity in the di-jet

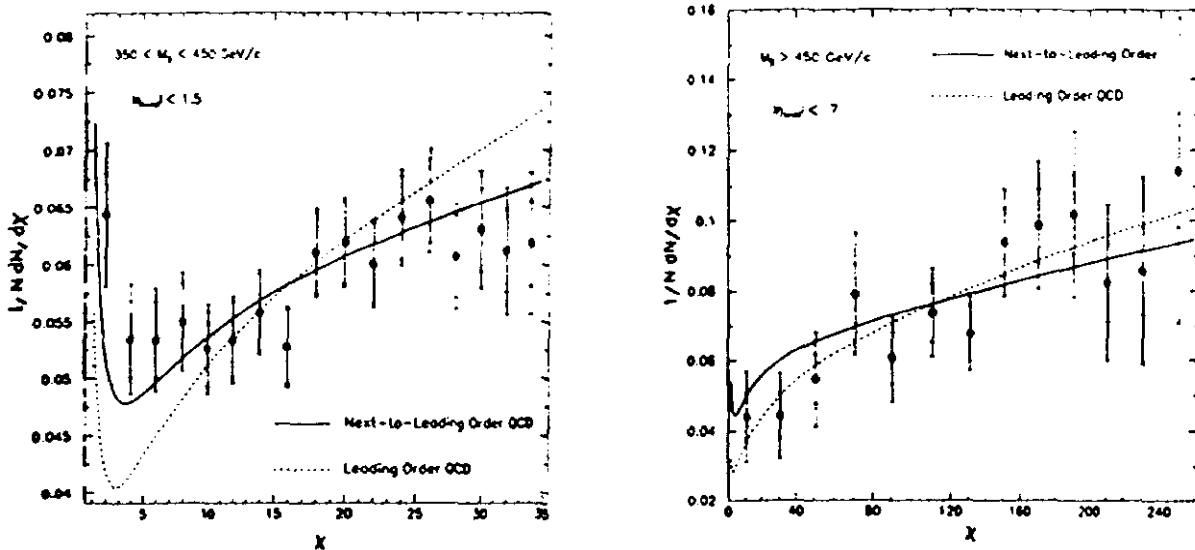


Figure 11. Angular distributions for di-jets for two ranges of di-jet mass and di-jet boost.

cm). Figure 11(a) shows the χ distributions for moderate mass di-jet pairs, together with LO and NLO QCD predictions^[17]; although the data errors are still quite large, mainly due to the residual uncertainties in the jet energy scale corrections, we see that the NLO corrections improve the fit. Figure 11(b) shows the distributions for large di-jet masses; these data extend the χ range to about eight times the value previously explored.

Another study of di-jets which explicitly probes the small- x gluon distribution was presented by CDF^[10]. Events with two jets at either the same or opposite rapidities were chosen; Fig. 12 shows preliminary data on the ratio of the same η to opposite η events as a function of $|\eta|$. This ratio is sensitive to the gluon structure function value at small x . Use of the ratio cancels some of the theoretical and systematic uncertainties, though some residual effects of jet energy smearing are still present. The enhancement around $|\eta| \sim 2.5$ tends to favor those structure function choices with larger $G(x)$ for small x .

A more complete study of NLO QCD for jets has been initiated by DØ^[14] using the full triple-differential cross-section $d^3\sigma/dE_T d\eta_1 d\eta_2$, where E_T is for the leading jet. Varying η_1 and η_2 selects different regions of x_1 and x_2 of the initial partons. Figure 13 shows a particular slice of these data for $E_T = 60$ GeV and $2.0 < |\eta_1| < 2.5$. In this region, the parton fractions vary from near 1 to 0.002. The comparison curve is a LO calculation which fails to reproduce the data at large $|\eta_2|$. With the expected theoretical NLO calculations, we look forward to improved information on distribution functions which can extend and complement deep inelastic scattering.

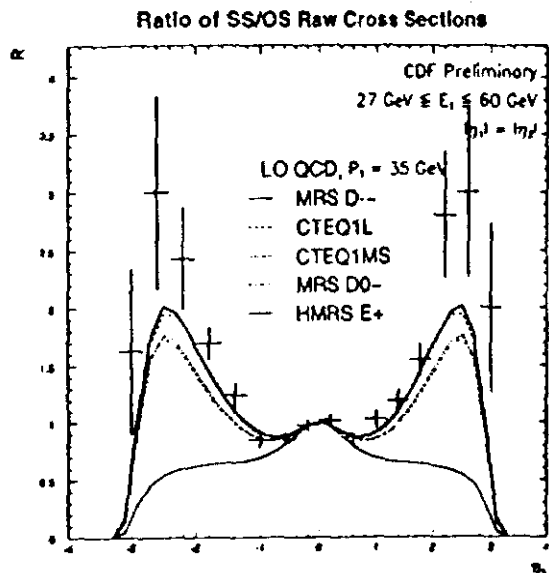


Figure 12. Ratio of di-jet events at equal η to those at opposite η vs. η .

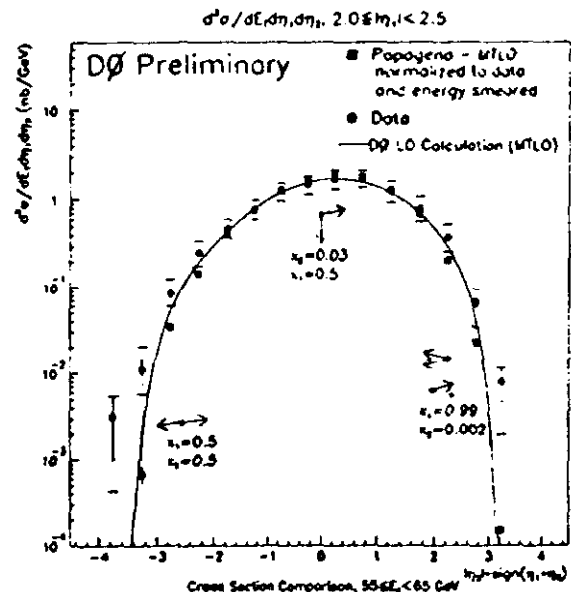


Figure 13. Triple differential cross-sections for the leading jet pair.

Three other new approaches to study multi-jet topologies were presented in this meeting. The first^[14] selects the two jets (over some E_T threshold) with the largest rapidity separation. In the presence of higher order QCD radiative and resummation effects^[18]

one expects the correlations in E_T between these two jets to wash out. The preliminary data agree qualitatively with the theory in showing such correlations for $\Delta\eta < 3$. The second approach^[14] selected three-jet events and directly compared observed topological parameters in the overall three-jet cm with $\mathcal{O}(\alpha_s^3)$ parton tree-level (PAPAGENO) and parton-shower Monte Carlos. For parameters such as the production angle of the stiffest jet, the angle between the plane containing the initial partons and the stiffest jet and the plane of the final three jet system, and the scaled jet energies, the agreement between data and PAPAGENO is quite good, while discrepancies exist for the shower Monte Carlos. The third quite preliminary new method follows the suggestion^[19] that gluon radiation probabilities will be enhanced in the region between two other jets; for example an enhancement is predicted between a high E_T jet and the beam fragment jet. Preliminary results^[20] show such enhancements in qualitative agreement with the HERWIG Monte Carlo which contains such color coherent effects.

A final rather specialized study of di-jet events was discussed using $D\bar{D}$ data^[20] in which the two observed jets ($E_T < 30\text{GeV}$) are separated by a gap in rapidity, $\Delta\eta_c$, within which there is no significant energy deposit in the EM calorimeter ($E_T < 0.20\text{ GeV}$ in a single tower). General arguments^[21] suggest that for subprocesses in which a colored object is exchanged, the distribution in $\Delta\eta_c$ should be rapidly falling. A colorless exchange state (e.g. Pomeron, γ , W/Z , ...) would result in a distribution which is approximately independent of $\Delta\eta_c$. The data shown in Fig. 14 shows the gap distribution, which after corrections, is consistent with the presence of a colorless exchange at the $< 10^{-2}$ level. Several experimental effects which can perturb the measured fraction of rapidity gap events to higher or lower values are still being studied so no claim was made for the unequivocal existence of colorless exchange.

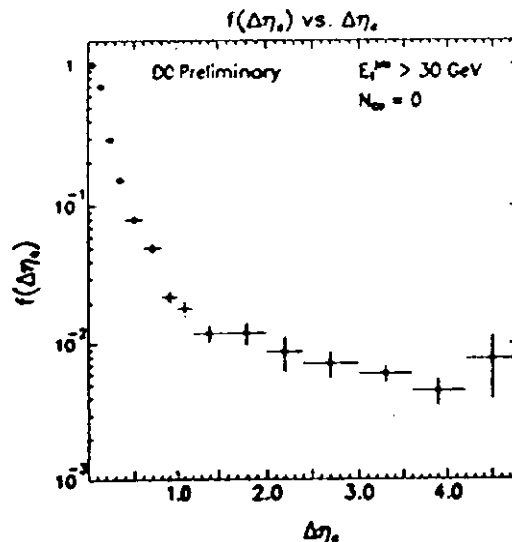


Figure 14. Measured distribution of events as a function of rapidity gap.

2.5 Direct Photon Production

Measurements of inclusive photons have been used as probes of the gluon structure function, since the Compton graph ($qg \rightarrow \gamma q$) gives a substantial contribution. New results for the photon cross-sections near $\eta = 0$ were presented by CDF^[10] and DØ^[12]. Both collaborations use the observation of conversions in preradiator material before the calorimeters; this method allows statistical separation of γ and π^0 and can be extended to as large p_T as statistics allow. CDF uses in addition a profile method which examines the lateral shower shapes in a special detector located near shower maximum in the EM calorimeter. Both experiments have extended this measurement to above 100 GeV/c and find reasonable agreement with NLO QCD calculations. The CDF data are shown in Fig. 15(a); Figure 15(b) shows the fractional deviation of these and the previous CDF results to the theoretical calculations^[22] with a range of scale parameter choices. Some systematic deviation from theory persists below 25 GeV/c. Extension of the photon cross-sections to large η is under study in the DØ collaboration; such results would give strong constraints on $G(x)$ at small x and would be of great value.

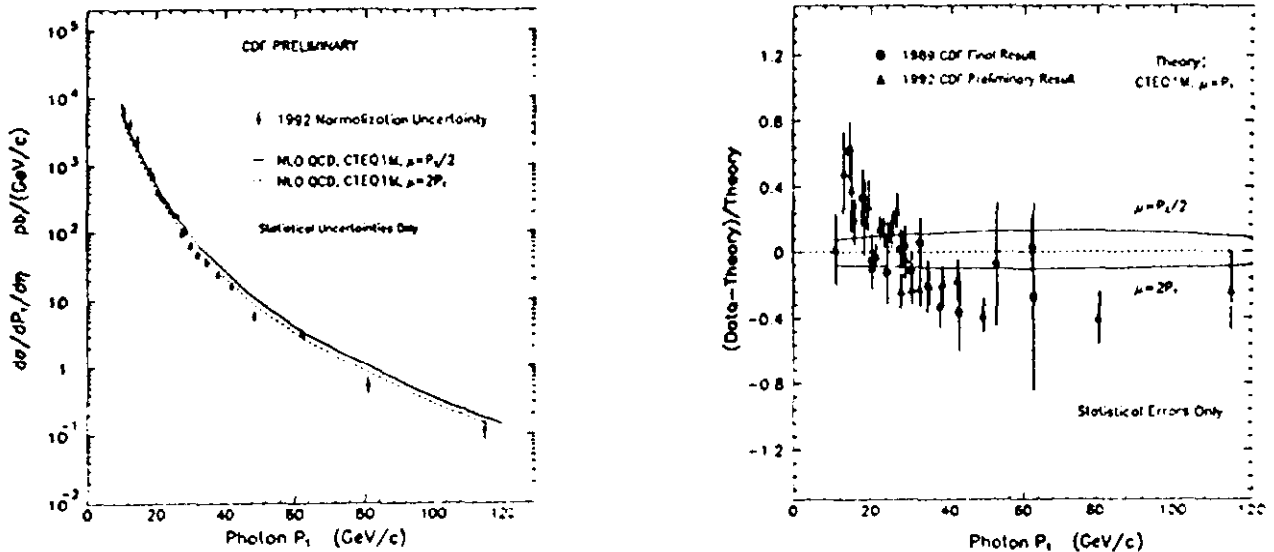


Figure 15. (a) CDF Inclusive photon cross-sections near $\eta=0$. (b) $(\text{CDF data} - \text{Theory})/\text{Theory}$ vs. p_T^γ .

CDF has studied the angular distribution for photon + jet production. These results have been published previously, but recent theoretical work improves the agreement between the data and NLO theory as shown in Fig. 16. In a separate study, the di-photon rates seen in CDF continue to exceed the NLO prediction by sizeable factors at large $m_{\gamma\gamma}$.

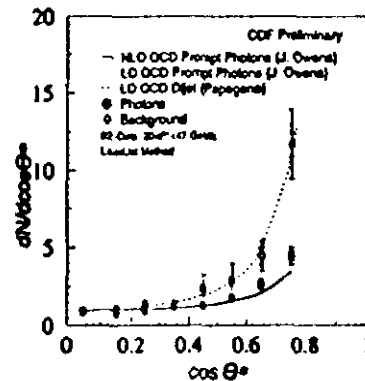


Figure 16. $\text{cm } \gamma\text{-jet}$ and di-jet angular distribution.

CDF showed a very interesting new result on the associated γ -charm production^[10]. The dominant production diagram is the Compton graph; isolation of this process thus gives a useful laboratory for study of both the gluon structure function, isolated from quark effects, and a probe of intrinsic charm within the proton. Charm detection was given both by observation of the $D^* \rightarrow D^0 \pi^+$ and by the semileptonic transition $c \rightarrow s \mu \nu$. These two measurements of $\sigma(\gamma c)$ give consistent results of about 700 pb, in agreement with theoretical expectations. Extension of this study should yield very interesting insights into the proton structure.

2.6 Production of b -Quarks

The production of b -quarks has been studied theoretically in some detail.^{[23] [24] [25]} In addition to the considerable interest in this cross-section for future hadron-collider b studies, the process is an interesting testing ground for QCD. The lowest order $b\bar{b}$ production processes (s-channel gluon diagrams or spin-1/2 t-channel quark exchange) are rivalled at large p_T by the $\mathcal{O}(\alpha_s^3)$ diagrams including the t-channel gluon exchanges with subsequent gluon splitting. Although earlier UA1 results^[26] were in reasonable agreement with NLO QCD at 630 GeV, more recent CDF results^[27] have tended to be roughly a factor of two higher than the theoretical central values. Several interesting new data were presented at this meeting which have helped illuminate this subject.

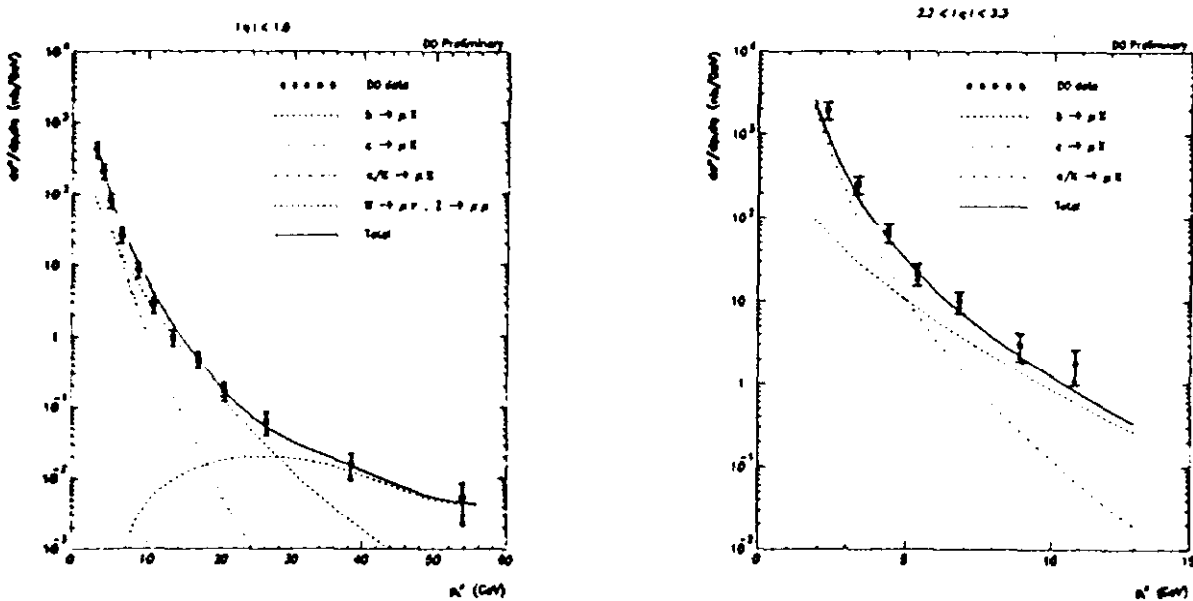


Figure 17. Inclusive muon cross-sections from DØ for central and forward muons.

The DØ collaboration^[28] presented inclusive muon cross-sections, without the unfolding to yield b cross-sections, which were compared to an approximate NLO calculation based on ISAJET. The ISAJET cross-sections for b 's agree well with the full NLO QCD values. Figure 17 shows these results for $|\eta| < 1.0$ and $2.2 < |\eta| < 3.3$, together with the expected decomposition of the b , c , π/K and W contributions. The cross-sections for

muons agree well with NLO QCD. It is also noteworthy that the data extend into the previously uncharted forward region where there is useful sensitivity to $G(x)$.

CDF has extended its inclusive b studies using exclusive $B \rightarrow J/\Psi K^\pm$, $J/\Psi K^{*0}$ measurements^[29]. The inclusive b cross-section above a minimum p_T deduced from these data are shown in Fig. 18. They exceed the NLO QCD calculation with standard structure functions, but can be accommodated with enhanced gluon contributions or alteration of the QCD scale. The CDF statistics for B^\pm production are now sufficiently large that a differential cross-section for $B + X$ can be produced. This result shown in Fig. 19 also exceeds the usual QCD calculation.

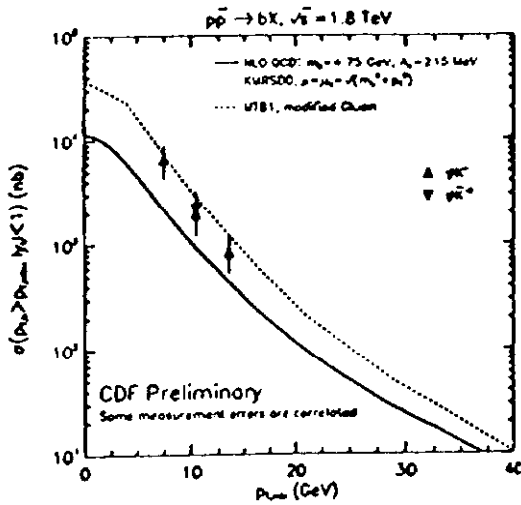


Figure 18. CDF integrated b cross-section.

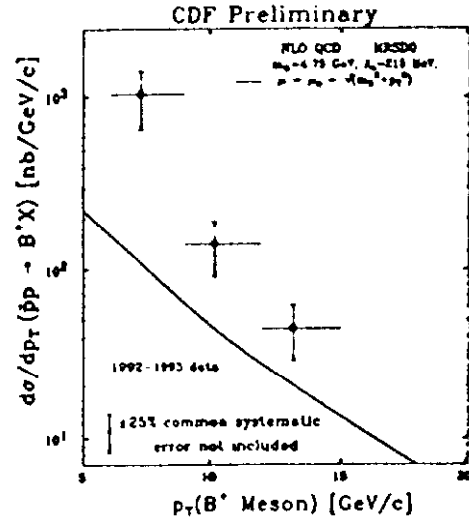


Figure 19. CDF differential inclusive B^\pm cross-section.

The UA1 muon data from 1988/89 have been analyzed in some detail, using new experimental signatures involving back-to-back dimuons and J/Ψ production. The inclusive b cross-sections extracted^[30] agree well with the NLO^[24] predictions. Using theoretical

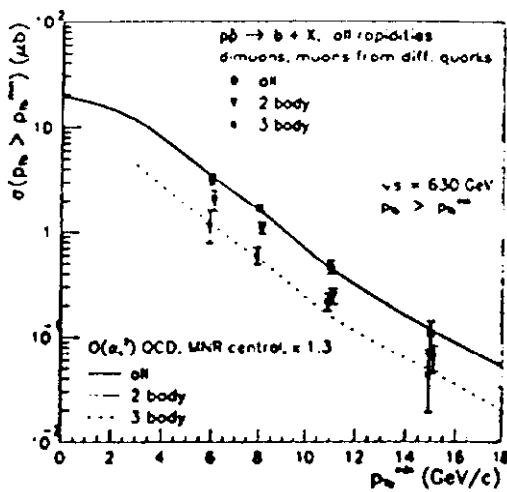


Figure 20. UA1 integrated b cross-section.

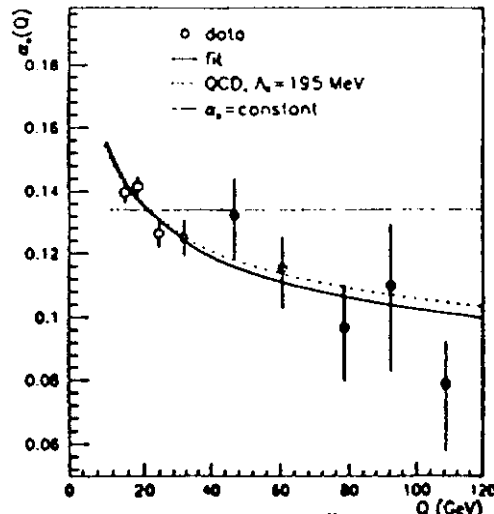


Figure 21. Dependence of α_s on q^2 scale from UA1.

guidance^[31] on the topological properties ($\Delta\phi_{\mu\mu}$ and dimuon separation in $\eta - \phi$) of the $2 \rightarrow 2$ and $2 \rightarrow 3$ processes, they extract these two components separately as shown in Fig. 20. From the NLO corrections to the $2 \rightarrow 2$ process, they fit α_s from their results. For central choices of structure functions and renormalization scale they obtain $\alpha_s(20 \text{ GeV}) = 0.145 \pm 0.018$, which scales to a value of 0.113 ± 0.011 at the Z . Separating their data into different p_T bins, it is possible to extract α_s as a function of q^2 and to demonstrate the running of α_s in a single experiment as seen in Fig. 21. These very nice results point the way for future decomposition of the inclusive b cross-section with higher statistics at the Tevatron.

2.7 W +jet production

The production of $W+n$ jets has an n -dependence of approximately $(\alpha_s(q^2))^n$, so measurement of the $(W + (n+1)\text{jets})/(W + n \text{ jets})$ ratio gives rather direct information on the strong coupling at $q^2 \sim m_W^2$. Using a recent NLO parton generator^[32] which parametrizes W production for 0 and 1 jets, DØ has parametrized the 0 and 1 jet cross-sections as a function of jet E_T^{min} , cone size and α_s . Comparing the ratio in the data to these parametrizations yields the result^[33]

$$\alpha_s(M_W^2) = 0.124 \pm .005(\text{stat}) \pm 0.006(\text{MC}) \pm 0.008(\text{str.fns})_{-0.022}^{+0.028}(\text{syst.}).$$

This first measurement of α_s at the Tevatron should improve with additional statistics and better understanding of the dominant error due to the jet energy scale.

3. Study of the b Quark

Studies of the b quark are expected to shed light on a variety of fundamental issues ranging from measurements of the CKM matrix elements ($\bar{B}_d^0 B_d^0$, $\bar{B}_s^0 B_s^0$ mixing), b -quark state lifetimes, study of the rich heavy-quark spectroscopy (B_s , B_c , Λ_b , Λ_{b_s} ...), rare b decay processes and consequent searches for new phenomena, and CP violation. Traditionally the province of e^+e^- colliders, the study of b -physics in hadron machines is now coming of age. Particularly with the advent of the silicon vertex detector (SVX) in CDF, measurements are being made in the complex hadronic environment with remarkable clarity and high statistics. The broad band character of hadronic production (many b -quark states produced in a single run) and the very large statistics afforded by the large cross-section ($\sigma \sim 30\mu\text{b}$) open possibilities not available to the e^+e^- machines.

3.1 $\bar{B}B$ Mixing

The DØ collaboration reported^[34] a new measurement of the $\bar{B}^0 B^0$ mixing parameter χ = relative probability for B^0 to evolve into a \bar{B}^0 . They measured the ratio of like-sign final state dimuons to unlike-sign pairs in the central region for $p_T > 2 \text{ GeV}/c$, and $m_{\mu\mu} > 6 \text{ GeV}/c^2$. Cuts on p_T^{μ} relative to a jet suppressed muons from π and K

decays, and to some extent the muons from direct and cascade charm decays which can contaminate the ratio. After Monte Carlo subtraction of the background contributions, they report $\chi = 0.13 \pm 0.02(\text{stat}) \pm 0.05(\text{syst})$ for mixture of B_d and B_s . This result is in good agreement with previous CDF, UA1 and LEP results. Combining this result with the ARGUS and CLEO studies of B_d mixing implies χ_s is greater than about 0.45, in accord with the constraints of other data and the Standard Model.

3.2 Study of the B_s Meson

CDF has updated their published result^[35] on the observation of the $B_s \rightarrow J/\Psi\phi$, with $J/\Psi \rightarrow \mu^+\mu^-$ and $\phi \rightarrow K^+K^-$ using about half of the 1992-93 data set.^[36] This analysis requires the presence of a displaced vertex for the B decay products to reduce the hadronic backgrounds. As shown in Fig. 22, they observe 21.6 ± 3.6 events over a background of about 10 and determine the B_s mass to be $5383.3 \pm 4.5 \pm 5.0 \text{ MeV}/c^2$. The $(B_s - B_d)$ mass difference of $94.5 \pm 4.6 \text{ MeV}/c^2$ is quite similar to the corresponding charm analog $(D_s - D_{u,d})$ difference of $99.5 \pm 0.6 \text{ MeV}/c^2$. The branching ratio has been determined by taking the ratio of events $(B_s \rightarrow J/\Psi\phi)/(B_d \rightarrow J/\Psi K^{*0})$ and normalizing to the CLEO measurement of the B_d branching ratio. The result, $\text{BR}(B_s \rightarrow J/\Psi\phi) = (9.0 \pm 2.0 \pm 2.5) \times 10^{-4}$ is obtained using the assumption of b -quark fragmentation ratios $(B_u : B_d : B_s) = 0.375 : 0.375 : 0.15$ and is dominated by the B_d branching ratio error. Further progress in this measurement should be forthcoming as CDF measures the fragmentation ratios by disentangling the B production rates through the semileptonic decays. The measured B_s branching ratio can be compared with heavy-quark theory predictions as for the B_d/B_u ; the predicted^[37] $\text{BR}(B_s \rightarrow J/\Psi\phi) = (12.5 \pm 5.0) \times 10^{-4}$, is in agreement with the data.

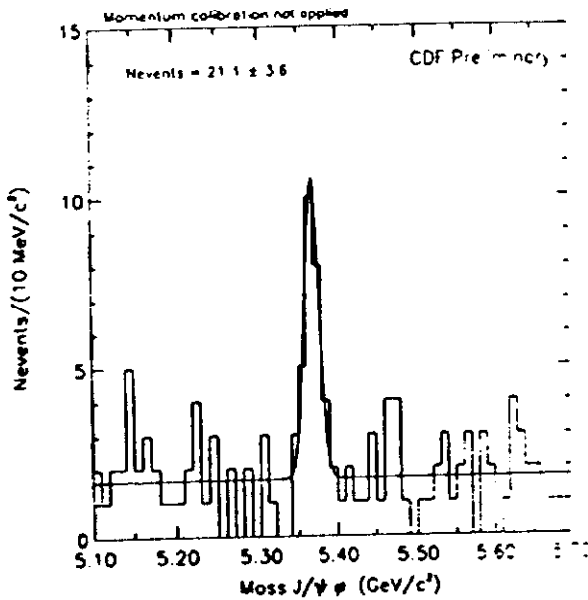


Figure 22. CDF dN/dM for $B_s \rightarrow J/\Psi\phi$.

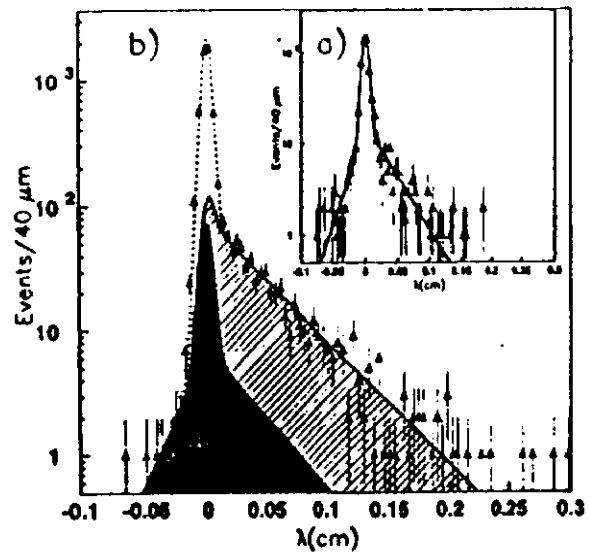


Figure 23. Decay length distribution for inclusive b 's.

3.2 *b*-Quark State Lifetimes

Measurements of the *b*-quark hadron lifetimes give good constraints on the CKM mixing matrix and test the heavy quark decay models. Whereas in the charm sector, non-spectator diagrams conspire with the simple *W*-emission graphs to give unequal lifetimes for the various *D* states, the large *b* mass is expected to reduce these interference effects for the *b* decays. CDF has measured lifetimes for a variety of *b* mesons^[38] through the use of the SVX. The CDF results are of comparable precision to those from the cleaner LEP environment and bode well for increased precision with added statistics. The inclusive *b* lifetime was determined by measuring the decay length of inclusive *J/ψ*'s and performing a three-component fit to non-*J/ψ* background, direct *J/ψ* from χ_c etc. and *J/ψ* from *b*'s. The conversion to a proper time is made with a Monte Carlo calculation of the momentum ratio of the *J/ψ* and the parent *b*. Figure 23 shows the decay length distribution for the sample; the background contribution is estimated from the *J/ψ* sidebands and the substantial excess at positive λ is due to the *b* \rightarrow *J/ψ* processes. Results are summarized in Table I.

Preliminary exclusive B_u and B_d lifetimes are determined from the decays $B_u \rightarrow \Psi K^\pm, \Psi K^{*\pm}$ and $B_d \rightarrow \Psi K_s^0, \Psi K^{*0}$, where $\Psi = J/\Psi$ or $\Psi(2S) \rightarrow J/\Psi \pi^+ \pi^-$, and *J/ψ* decays into $\mu^+ \mu^-$. Results are given in Table I.

A noteworthy new result from CDF^[38] is the measurement of the B_s lifetime through the semileptonic decay $B_s \rightarrow D_s^+ (\rightarrow \phi \pi^+) + \ell^- \nu$. The leptons are required to be isolated and have $p_T > 6$ GeV/c. SVX tagging is required for the lepton and at least two other tracks. They require $3.0 < M(\ell^- D_s^+) < 6.0$ GeV/c² to reject backgrounds, and use the $(\ell^- D_s^+)$ momentum and a Monte Carlo correction to give an approximation to the B_s momentum. The distribution of events with proper time is shown in Fig. 24; a clear excess at positive cr is observed. Backgrounds are estimated from wrong-sign combinations. Lifetime results are given in Table I.

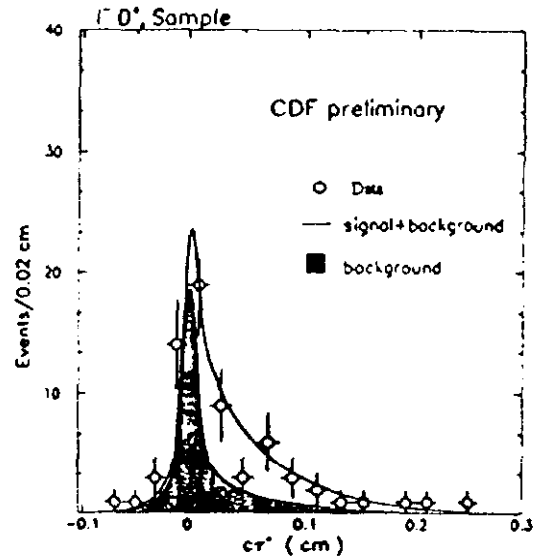


Figure 24. Proper time distribution for semileptonic B_s decays.

Table I. b Meson Lifetimes

Sample	CDF result (ps)	World Average (ps)
Inclusive b	$1.46 \pm 0.06(\text{stat}) \pm 0.06(\text{syst})$	1.52 ± 0.023
B_u	$1.63 \pm 0.21 \pm 0.16$	1.66 ± 0.12
B_d	$1.54 \pm 0.22 \pm 0.10$	1.54 ± 0.11
$[\tau_{B_u}/\tau_{B_d}]$	$1.06 \pm 0.20 \pm 0.12$	1.06 ± 0.12
B_s	$1.54^{+0.42}_{-0.34} \pm 0.11 \pm 0.12$	1.42 ± 0.21

4. Electroweak Bosons

Much new information on Electroweak physics was presented in this workshop which extends the beautiful results from LEP. The hadron colliders are uniquely positioned to explore the properties of the W boson and to probe the full set of trilinear gauge boson couplings.

4.1 Production Cross-sections

The measurement of

$$R = (\sigma B)_W / (\sigma B)_Z = (\sigma_W / \sigma_Z) \times (\Gamma(W_{lv}) / \Gamma(Z_{ll}) \times (\Gamma_Z / \Gamma_W),$$

together with the theoretical cross-sections and partial widths and the LEP total Z -width, yields accurate values for the W width. This information can be used to probe for unseen W decays - in particular the possible $W \rightarrow tb$ with $t \rightarrow$ unseen final states. New measurements of R were presented at this conference from both CDF and DØ. These are summarized in Table II. With these data, CDF^[39] gives the limit $m_t > 62$ GeV and DØ^[33] gives $m_t > 56$ GeV (both at 95% confidence level).

Table II. W/Z cross-sections

Data set	$(\sigma B)_W$ (nb)	$(\sigma B)_Z$ (nb)	R	Γ_W (GeV)
CDF e			$10.65 \pm 0.36 \pm 0.27$	$2.03 \pm 0.07 \pm 0.06$
CDF μ			$12.38 \pm 0.63 \pm 0.45$	1.80 ± 0.11
DØ e	$2.25 \pm 0.03 \pm 0.10$	$0.21 \pm 0.01 \pm 0.02$	$10.70 \pm 0.60 \pm 0.50$	$2.05 \pm 0.11 \pm 0.11$
DØ μ	$2.00 \pm 0.07 \pm 0.48$	$0.20 \pm 0.02 \pm 0.05$	$10.0 \pm 1.1 \pm 2.4$	
Std.Model				2.067 ± 0.021

4.2 Gauge Boson Couplings

The trilinear coupling of the Electroweak gauge bosons is completely specified in the Standard $SU(2) \times U(1)$ Model, so that exact predictions exist for the production and kinematic distributions of gauge boson pairs^[40]. In general, the trilinear couplings arising in the s -channel diagrams can interfere with quark exchange or radiative decay diagrams to give characteristic angular distributions. The CP-conserving anomalous couplings, $\Delta\kappa$ and λ , can be non-zero in extensions to the SM and, if present, will modify the rates and distributions. The largest gauge boson pair production is for $W\gamma$. CDF contributions^[39] to this workshop updated the $W\gamma$ study and added information about the $Z\gamma$ process with W/Z decays into electrons or muons, using 4 pb^{-1} of data from the 1989 run. The CDF data sample contains 8 (5) events in the $W(e)\gamma$ ($W(\mu)\gamma$) channels and about 1:1 signal to background in each. There are two events in each lepton channel for the $Z\gamma$ study. $D\bar{O}$ ^[41] reported a measurement of $W\gamma$ production in both electron and muon channels using 15 pb^{-1} from the recent run. They observe 10 events in each channel with backgrounds of about 4 events each, due to W +jet with a jet faking a lepton or contamination from $Z \rightarrow \mu\mu + \gamma$. With the small statistics in either experiment only the total rate is used to extract limits on $\Delta\kappa$ and λ , but with the data from the next run much more sensitive studies should be possible using the p_T^7 and $\cos\theta_{W\gamma}$ distributions. The 95% contour limits in the $\Delta\kappa$ - λ plane for the $D\bar{O}$ data are shown in Fig. 25. The present anomalous coupling limits are given in Table III.

Table III. Anomalous Trilinear Gauge Boson Coupling 95% Limits

Data set	$\Delta\kappa(\lambda = 0)$	$\lambda(\Delta\kappa = 0)$
CDF ($\mathcal{L} \sim 4\text{pb}^{-1}$)	$-6.5 < \Delta\kappa < 7.0$	$-3.1 < \lambda < 3.1$
$D\bar{O}$ ($\mathcal{L} \sim 15\text{pb}^{-1}$)	$-2.5 < \Delta\kappa < 2.6$	$-1.2 < \lambda < 1.1$
Standard Model	0	0

CDF reported a single tri-electron event which is a candidate for WZ pair production; inclusion of this channel together with $Z(\nu\nu)\gamma$ and WW , and measurement of the p_T and angular distributions in the next run should make substantial improvement in the SM Electroweak coupling tests.

4.3 W Decay Asymmetry

The forward-backward asymmetry of the charged leptons with respect to the initial proton direction in $\bar{p}p$ collisions occurs through the combination of the difference in $u(\bar{u})$ and $d(\bar{d})$ distributions in the initial hadrons and the $(V - A)$ character of the charged current decay. Since the weak interaction properties are well-established, measurement of this asymmetry primarily illuminates the quark structure of the proton. Since W 's are

produced through $q\bar{q}$ fusion, the asymmetry $A(\eta_\ell)$ is mainly sensitive to the slope of the d/u ratio as a function of x . DØ^[42] and CDF^[43] both reported results on the W asymmetry. Figure 26 shows the CDF electron and muon data, together with the predictions from NLO QCD with several parton distribution functions. The data are becoming accurate enough to discriminate among some of these choices, even when the deep-inelastic scattering data do not.

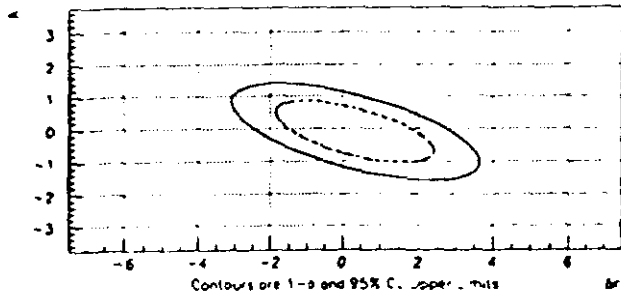


Figure 25. DØ Limits on anomalous couplings $\Delta\kappa$ and λ .

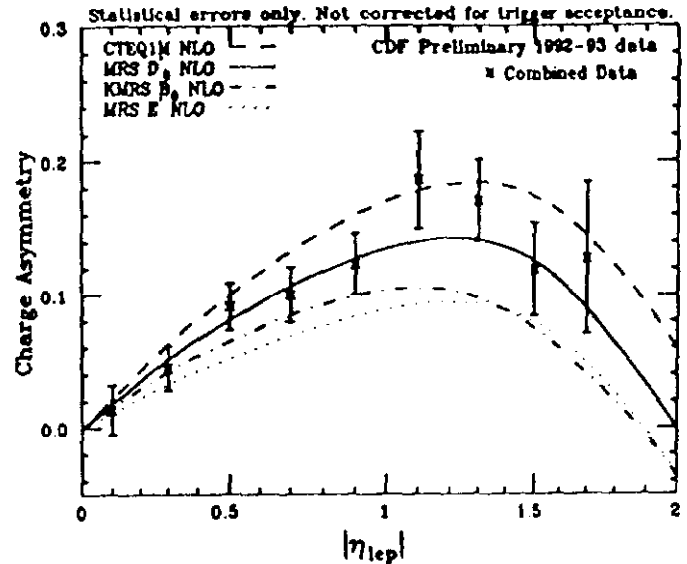


Figure 26. CDF W charge asymmetry vs. η_ℓ .

4.4 W Mass Measurement

The precise measurement of m_W is one of the cornerstones of hadron collider physics. Together with the accurate values of the Z mass, width and decay asymmetries, accurate m_W permits an overconstrained fit of the fundamental Electroweak parameters and delimits the range of possible top quark masses within the SM framework. In future, with the addition of an accurately known top mass, these Electroweak measurements can give constraints on possible Higgs masses.

Both CDF^[44] and DØ^[45] reported new values for m_W in this meeting, using electrons in the central ($|\eta| < 1$) region in conjunction with large missing E_T to signal the presence of the neutrino. The quantity measured is the transverse mass, $m_T^2 = 2E_T^e E_T^\nu (1 - \cos\phi_{e\nu})$. Careful attention is needed to determine accurately the hadronic and electromagnetic energy scales for the detector from which the neutrino and W p_T 's are inferred. In both experiments, the companion samples of $Z \rightarrow e^+e^-$ are used to study these systematic effects. The Z event properties are similar to those for the W , but with both decay leptons observed, the transverse momentum balance of the dilepton and recoiling hadronic system can be carefully measured and corrected.

An accurate overall energy scale is also required. In the CDF case, the ultimate

standard is the magnetic tracking measurement of the J/Ψ and the observed E/p for the electrons from W decay. In the non-magnetic $D\emptyset$ detector, the energy scale is fixed by the measurement of the Z in its di-electron decay mode. Since the $D\emptyset Z$ mass is about 4.5% below the measured LEP value, independent evidence must be found to support the assumption that the energy scale is linear. Two methods using experimental data from the collider run were reported; the first uses a $J/\Psi \rightarrow ee$ signal to establish the linearity. The second uses the measured Z itself, using the range of electron energies observed in the detector from high $p_T Z$'s. With the detector response functions determined, the data are compared with an ensemble of Monte Carlo distributions of varying m_W (and in the case of CDF, Γ_W). $D\emptyset$ has also included the effects of additional interactions during the same beam-crossing in this calculation. Minimization of the likelihood function of the Monte Carlo difference from the data distribution yields the best m_W value. Figures 27 and 28 show the quality of this best fit for the m_T distributions; in each case the fit is excellent, including the tails of the distribution. The measured p_T^e , p_T^ν and p_T^W distributions are similarly well measured.

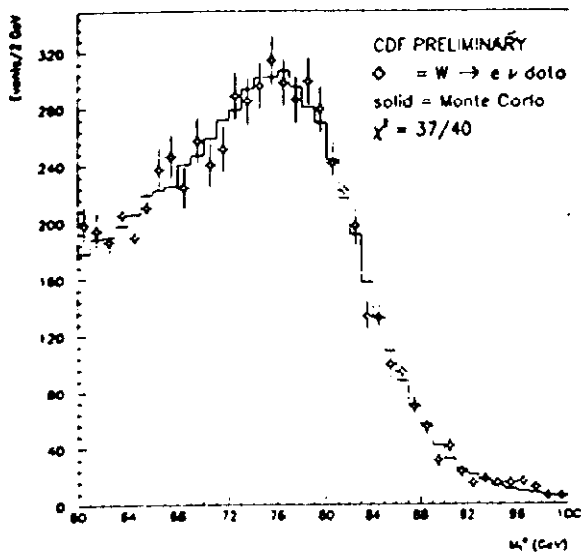


Figure 27. CDF best fit m_T distribution.

$D\emptyset$ Preliminary: $W \rightarrow e \nu$ Decays (CC only)

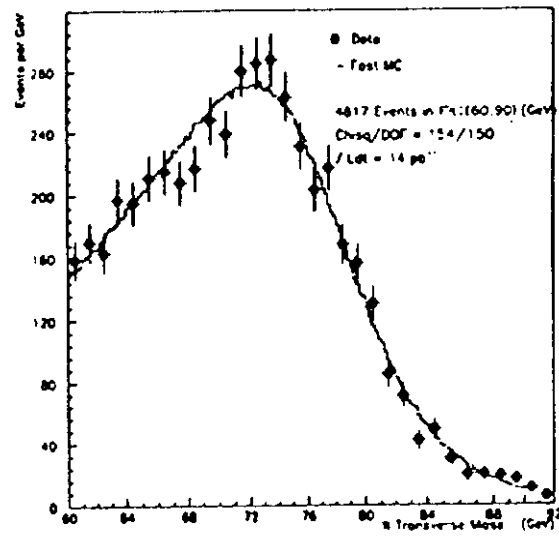


Figure 28. $D\emptyset$ best fit m_T distribution.

The CDF preliminary determination using data from the 1992-3 run gives $m_W = 80.47 \pm 0.15(\text{stat}) \pm 0.25(\text{syst})$ GeV with Γ_W fixed at 2.1 GeV. The systematic error contains the 130 MeV error due to the energy scale uncertainty. Allowing Γ_W to float gives an insignificantly different value. The $D\emptyset$ preliminary result is $m_W = 79.86 \pm 0.16(\text{stat}) \pm 0.20(\text{syst}) \pm 0.31(\text{scale})$ GeV. The last $D\emptyset$ error is a conservative estimate of the uncertainty in the energy scaling. In both cases the dominant systematic errors are controlled by the size of the Z sample and thus will be reduced with more data.

The new combined world data on m_W taken from UA2^[46], CDF(1989)^[47], and the new CDF and $D\emptyset$ results gives $m_W = 80.21 \pm 0.18$ (all errors in quadrature). This combined

value is plotted in Fig. 29, together with the constraints in the m_W - m_t plane from the LEP Z mass, total and leptonic widths, and asymmetries. The new W mass measurement is now comparable with the LEP measurements in constraining the top mass.

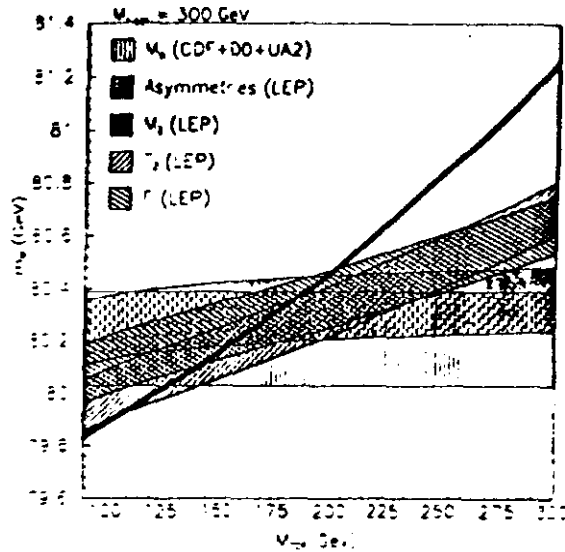


Figure 29. Allowed regions in m_W vs. m_t from the world average m_W and LEP Z measurements.

5. Searches for Phenomena outside the Minimal Standard Model

Observation of particles outside the framework of the Minimal Standard Model would constitute the simplest and most dramatic evidence for the existence of new physics. Alas, no such evidence was reported at this conference.

5.1 Excited Quarks

Possible excited quark states would directly show the quarks as composite objects. Such particles should decay to the ground state quarks through emission of a vector boson (g , γ , W , or Z). CDF has searched for excited quarks (q^*) in both the jet- W (e or μ) and jet- γ channels^[48]. Comparing the experimental upper limits in these channels with a theoretical model calculation^[49], they obtain excluded regions for the q^* mass of $80 < m_{q^*} < 460$ GeV ($q\gamma$); $150 < m_{q^*} < 530$ GeV (qW); and $80 < m_{q^*} < 540$ GeV (combined). This result limits possible quark compositeness in a rather different way from the search for deviations from expected high p_t jet cross-sections, but the compositeness mass scale probed is similar.

5.2 Heavy Gauge Bosons

Models with extended gauge symmetries permit the existence of gauge bosons beyond the standard W and Z . Both CDF^[43] and DØ^[42] have extended the search for the W' and Z' in electron decays, assuming standard model couplings to leptons. For the high

masses studied, the backgrounds from conventional sources are small. The largest mass events seen are at about 300 GeV. The 95% confidence level limit for W' from $D\bar{O}$ is 600 GeV. The 95% confidence level limits for Z' from CDF and $D\bar{O}$ are 495 GeV and 440 GeV respectively.

5.3 Supersymmetric Particles

The existence of a rich spectrum of particles, dual to the ordinary fermions and bosons, is predicted by a large family of supersymmetric theories^[50]. Although the Minimal Supersymmetric Model (MSSM) has several free parameters which complicate the search, certain regularities in the mass scale are natural.

The charged Higgs bosons, H^\pm , are partners of the minimal Higgs H^0 in MSSM and decay into heavy fermion pairs ($\tau\nu$, $c\bar{s}$, ...). If the top is light ($m_t < m_W - m_b$) and a lighter H^\pm exists ($m_{H^\pm} < m_t - m_b$), such a top quark would have gone unobserved in a conventional search. CDF reported a search for this decay sequence in 4.1 pb^{-1} ^[51], in which the H^\pm is sought in the $(\tau\nu)$ mode and $\tau \rightarrow (1 \text{ or } 3 \text{ particles}) + \nu$. The H^\pm branching ratio is controlled by $\tan\beta$, the ratio of vacuum expectation values in MSSM. From data on $B^0 - \bar{B}^0$ mixing, $\tan\beta$ is expected to exceed 0.5 and hence $\text{BR}(H^\pm \rightarrow \tau) > 0.3$. The search required, in addition to the τ jet, a second jet with $E_T > 12 \text{ GeV}$, and $\cancel{E}_T > 25 \text{ GeV}$. The dominant background from $W \rightarrow \tau + \text{jets}$ was found to account for all observed events, and a null result was derived *jointly* for H^\pm and top. Figure 30 shows the region of $m_{H^\pm} - m_t$ space that is ruled out for various hypothesized values of $\tan\beta$.

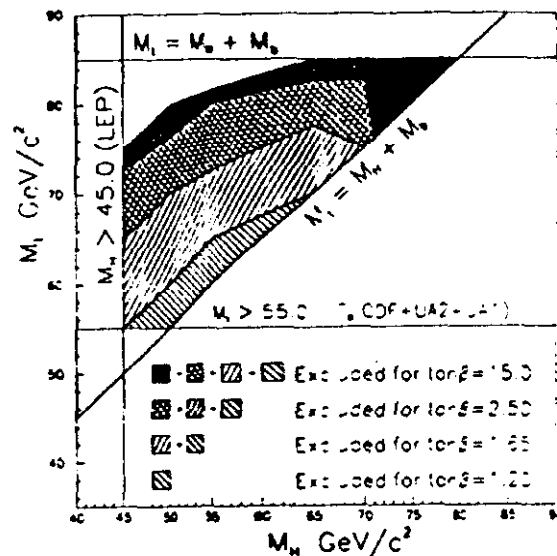


Figure 30. Disallowed regions from CDF in m_{H^\pm} vs. m_t .

Searches for the supersymmetric partners of the W, Z were conducted by both CDF and $D\bar{O}$. In the MSSM, the gaugino spectrum contains a pair of \tilde{W} 's and four \tilde{Z} 's. The lightest \tilde{Z} , \tilde{Z}_1 , is the lowest supersymmetric particle formerly called the photino. The production diagrams for \tilde{W} 's and \tilde{Z} 's are fully prescribed in the MSSM, once the masses are

known. The decay characteristics are model dependent, but are expected to contain a large proportion of leptons, through decays such as $\widetilde{W} \rightarrow \widetilde{Z}_1 W (\rightarrow \ell \nu)$ or $\widetilde{Z}_2 \rightarrow \widetilde{Z}_1 Z (\rightarrow \ell^+ \ell^-)$. In MSSM, the masses of \widetilde{W}_1 and \widetilde{Z}_2 are approximately equal, and for a broad class of model parameters, $m_{\widetilde{Z}_2} \sim (3 - 4) \times m_{\widetilde{W}_1}$. DØ^[52] and CDF^[53] searched for evidence of gaugino production in all four trilepton channels. They obtain limits on the cross-section for their production which, given theoretical model calculations^[54], can be converted to mass limits which depend upon the choice of free SuSy parameters. For a specific set of choices^[53] CDF finds that a small previously allowed region in $m_{\widetilde{Z}_2} - m_{\widetilde{W}_1}$ space can be excluded. The DØ results shown in Fig. 31 indicate the cross-section upper limits for gaugino production vs. \widetilde{W}_1 mass, together with the MSSM predictions for a range of decay branching ratio assumptions. A significant portion of the parameter space for low mass \widetilde{W} 's has been excluded.

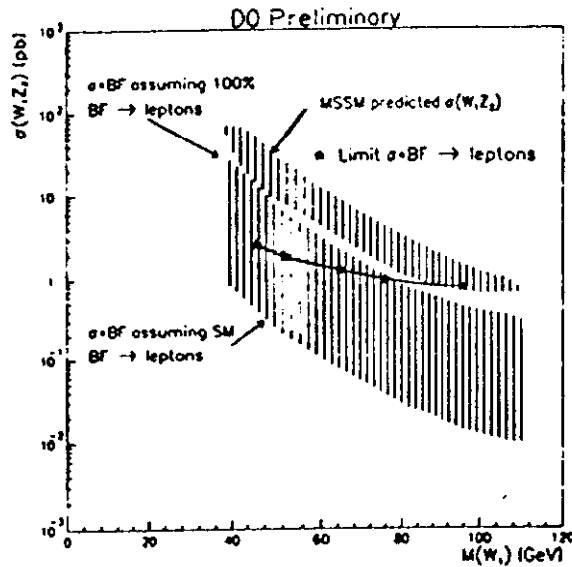


Figure 31. DØ cross-section limits and theoretical predictions for gaugino production vs. \widetilde{W}_1 mass.

5.4 Leptoquarks

In models with composite Higgs or extended gauge groups, new flavor degrees of freedom exist which result in a new heavy particle spectrum^[55]. One of the most striking of these possibilities experimentally is the leptoquark which carries both lepton and quark quantum numbers. DØ presented a search for the production of first generation leptoquarks^[52] which are expected to decay into e +quark or ν +quark. This analysis is independent of the unknown quark-lepton coupling strength since, in \bar{p} - p collisions, the leptoquarks are pair produced by ordinary QCD mechanisms. The experimental signatures in the $ee+2$ jets and $e\nu+2$ jets are quite clean once the backgrounds from $W/Z+2$ jets are removed. Figure 32 shows the resulting limit on first generation leptoquark mass as a function of the branching fraction of the leptoquark into e or ν final states. These limits improve upon the previous CDF and LEP limits. The HERA experiments have set limits on leptoquark production through s -channel e +quark production of about 180 GeV

under the rather restrictive assumption that the quark-lepton coupling is the same as the Electroweak coupling.

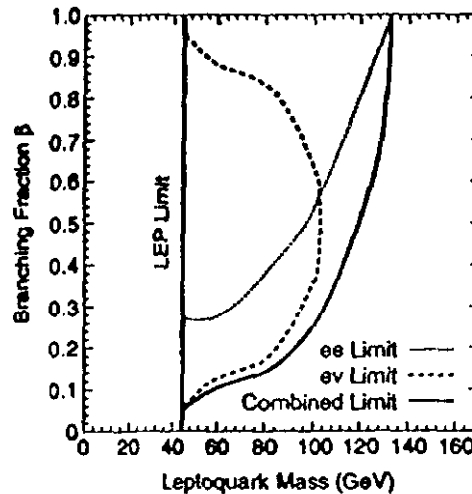


Figure 32. $D\bar{0}$ Mass Limits for first generation leptoquarks.

6. Search for the Top Quark

As is well known, the top quark is the last particle in the Minimal Standard Model (save the Higgs) for which no direct evidence exists. As in the search for the Yeti – the Abominable Snowman – rumors of the sighting of the top have circulated widely, but without confirmation. The reports from $D\bar{0}$ and CDF in this conference gave no new substance to these rumors, but have expanded the territory within which the top does not exist.

For the heavy top quark now expected, the produced t and \bar{t} should decay into $W + b$. (Reduction of the possible loophole for $m_t < m_W$ was discussed above in Sections 4.1 and 5.3.) The different search channels are distinguished by the W decays into $(q\bar{q}, e\nu, \mu\nu, \text{ or } \tau\nu)$. Results were presented in this meeting for the dilepton modes ($ee, \mu\mu, \text{ and } e\mu$), single lepton modes (e, μ) and the all jets (no leptons) mode.

6.1 Top Search in the Dilepton Modes

With both W 's decaying leptonically, the basic dilepton top signature of 2 leptons, \cancel{E}_T and 2 jets is distinctive. But with $\mathcal{O}(10^{12})$ inelastic collisions in the present exposures, QCD effects which modify the jet characteristics, detector imperfections, and some real physics backgrounds, the search for $t\bar{t}$ in the dilepton mode remains a formidable challenge. The kinematic selections, cuts, efficiencies for top, and estimated backgrounds for CDF^[66] and $D\bar{0}$ ^[57] are shown in Table IV. Each experiment has observed two events. The limits on the top quark mass are discussed in the next section.

Table IV. CDF and DØ Dilepton Top Searches

Channel B.R.	CDF			DØ	
	ee	$\mu\mu$	$e\mu$	ee	$e\mu$
B.R.	1.23%	1.23%	2.47%	1.23%	2.47%
$\int \mathcal{L} dt$	71.4 pb ⁻¹			15.2 pb ⁻¹	
p_T^l (GeV)	> 20			> 20	> 15
\cancel{E}_T (GeV)	> 25			> 25	> 20
n_{jets}	> 2				> 1
E_T^{jets} (GeV)	> 10				> 15
Mass Cuts	$\Delta m(Z - ee)$ >15 GeV	$\Delta m(Z - \mu\mu)$ >15 GeV		$\Delta m(Z - ee) > 12$ (if $E_T < 40$)	
Other Cuts	Opposite sign dileptons lepton isolation (<3 GeV in $\Delta R = 0.25$) $\Delta\phi(\cancel{E}_T, \ell)$ and $\Delta\phi(\cancel{E}_T, jet) < 20^\circ$ if $\cancel{E}_T < 50$				$\Delta R_{e\mu} > 0.25$
eff($m_t=120$)	10% (avg)			19%	17%
eff($m_t=140$)	13% (avg)			19%	19%
eff($m_t=160$)	15% (avg)			20%	19%
N($m_t=120$)	3.7 total			1.4	2.5
N($m_t=140$)	2.2 total			0.6	1.2
N($m_t=160$)	1.3 total			0.3	0.6
N_{blind}	0.16	0.16	0.23	0.5	1.1
$N_{est}(data)$	0	0	2	1	1

The single DØ surviving event in the $e\mu$ channel is sufficiently far from the cut thresholds (doubling lepton and missing E_T and doubling the number of required jets leaves this event still far from the cuts) that kinematic analysis was performed under the hypothesis of $t\bar{t}$ production. Assuming a value for m_t and making a specific association of the jets in the event as b quarks, a OC fit can be made to the full kinematics^[58] They weight each solution with parton distribution functions and cross-sections and lepton decay distributions, and sum these weights over all jet and lepton combinations. This single event probability distribution is shown in Fig. 33(a); the shoulder at low mass derives from taking an energetic jet in this event as initial state radiation. The probability curve for this single event peaks in the 140 - 150 GeV region. Figure 33(b) shows a similar analysis (with somewhat different weight function); the solid curve is the probability similar to that of Fig. 33(a). The dotted curve is the result of convoluting the observation of the most likely m_t for the single event with an ensemble of Monte Carlo top event distributions to get a likelihood curve. Although such kinematic analyses are not by themselves able to

discover the top, they will clearly play a role in establishing the validity of a signal, and will aid in determining the mass of the top once discovered.

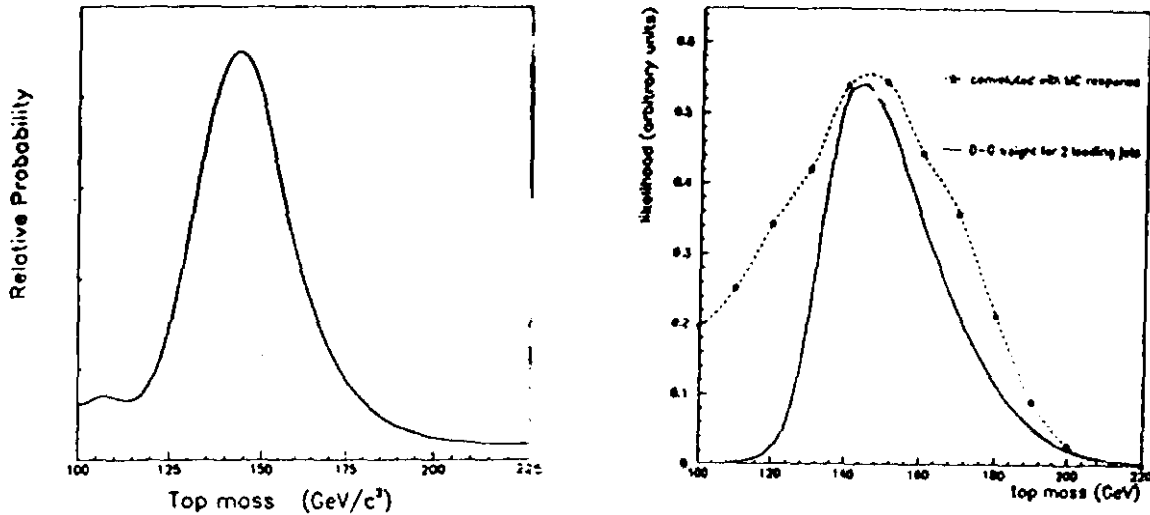


Figure 33. Probability distribution for the $DØ$ $e\mu$ event under the top hypothesis.

6.2 Top Search in the Single Lepton Modes

The $W+4$ jets production (with $W \rightarrow l\nu$) gives sufficiently large background for the $t\bar{t}$ production with decay into lepton, \cancel{E}_T , and four jets that special suppression techniques must be adopted. In addition, multijet QCD events can sometimes provide lepton and \cancel{E}_T signatures resembling $t\bar{t}$.

A topological method for background suppression was presented by $DØ$ ^[59]; the imposition of \cancel{E}_T is itself quite effective at reducing the QCD backgrounds but does little to eliminate W +jets. However, they observe that the aplanarity variable (the smallest eigenvalue of the momentum tensor of final state jets and W) usefully separates the W +jets from top. With a cut on aplanarity $\mathcal{A} > 0.075$, $E_T^e > 20$ GeV, $\cancel{E}_T > 20$ GeV, ≥ 3 jets with $E_T > 15$ GeV), and a requirement that there be at least one solution with $|m_{W+jet} - m_{other\ 3\ jets}| < 25$ GeV, they find no surviving events in the e +jets sample in 13 pb^{-1} and expect a background of 2.1 ± 0.3 . The expected number of $t\bar{t}$ events (140 GeV) is 2.1 ± 0.9 . A similar analysis^[59] for the μ +jets yields one surviving event in 11 pb^{-1} with expected backgrounds and $t\bar{t}$ (140 GeV) of 2.0 ± 0.6 and 1.7 ± 0.3 events respectively.

One of the prime techniques for enhancing the top signal is b -jet tagging. The $t\bar{t}$ events are expected to have two b 's whereas the W +jets process is not enriched in b 's^[23]. CDF presented two b -tagging analyses^[60]. Both start with a sample selected using $p_T^l > 20\text{ GeV}$, $\cancel{E}_T > 20$ GeV and ≥ 3 jets. In the first of these, the SVX was used to flag jets whose tracks are displaced from the primary vertex. Samples enriched with b jets were used to study the b tagging efficiency. A QCD sample was used to study the resolution in vertex separation. This analysis is in a preliminary stage, but the technique is very promising. Three events

remain in 21.4 pb^{-1} after requiring a three standard deviation cut on the impact parameter and the two-dimensional decay vertex separation. The background was estimated to be between 0.55 and 1.2 events; for 140 GeV top they would expect 4.7 ± 1.8 events.

Tagging b 's can also be accomplished by identifying the soft leptons from b semileptonic decay. With two b 's per $t\bar{t}$ event, two semileptonic decay channels (e and μ), and the additional possibility for observing leptons from the cascade charm decay, this method also has appreciable efficiency. The tagging leptons are moderately low in p_T and are not isolated from neighboring jet activity. CDF has performed a soft lepton tag analysis^[60] for both e and μ ($p_T > 2 \text{ GeV}$) and the same basic event sample as discussed above. They report 2 events surviving in 10 pb^{-1} , with an estimated background of 1.8 ± 0.2 events and an expected signal ($m_T = 140 \text{ GeV}$) of 2.0 ± 0.4 . DØ has also performed a muon tag analysis of the e +jets sample. With relaxed cuts on aplanarity and \cancel{E}_T , but requiring a soft, non-isolated muon, they find 2 events (13 pb^{-1}) with background and top signal (140 GeV) of 2.0 ± 0.6 and 1.7 ± 0.3 events respectively.

The limit on the top quark mass can be obtained from the analyses presented here, in conjunction with theoretical cross-sections for $t\bar{t}$ production. For this analysis, each experiment takes the conservative approach of neglecting backgrounds so that the observed events are attributed to top. Poisson distributions in the number of observed events and errors in acceptances and luminosity are combined to give a 95% upper limit on the $t\bar{t}$ cross-section as a function of mass. The intersections of this curve with the lower limit of a NLO

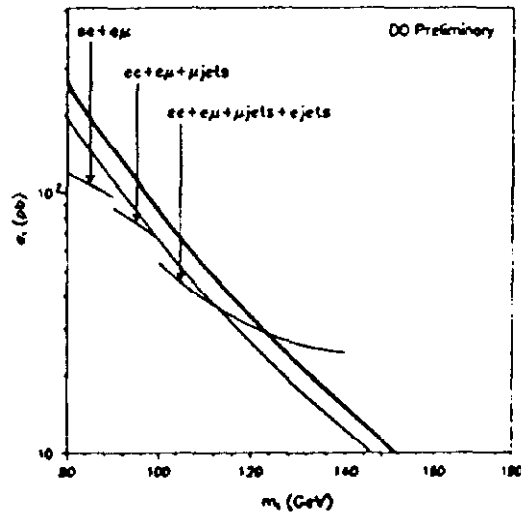


Figure 34. Upper limit cross-section and top mass limit from the DØ experiment.

calculation^[61] and an approximate lower limit of a NNLO calculation^[62] are shown in Fig. 34 for the DØ analyses (dilepton, lepton + jet with and without b -tag). The DØ conservative limit (no background subtraction, 95% experimental upper limit and lower limit theoretical cross-section) yields $m_t > 124 \text{ GeV}$ from the NNLO curve^[62] and

$m_t > 113$ GeV using the NLO curve^[61]. CDF has reported^[63] $m_t > 113$ GeV using the NLO curve and the dilepton analyses alone. Preliminary calculations combining these CDF and $D\bar{D}$ results give a limit of about 129 GeV for the NNLO cross-section. Further increases in the top quark mass limit with the present analyses may be slow – the searches are beginning to produce events in the signal region!

6.3 Top Search in the All Jets Mode

The decay mode $t\bar{t} \rightarrow$ all jets is the largest branching ratio (44%) and poses the greatest challenge due to the huge QCD backgrounds. CDF has reported^[64] a very preliminary Monte Carlo study of this mode in which the kinematic cuts for six jet events (E_T^{jets} , \cancel{E}_T , jet centrality) are tightened relative to the leptonic channels. An SVX tagged secondary vertex is required as well. Finally, these events are subjected to a neural network classifier in order to discriminate the $t\bar{t}$ events from QCD multi-jets based on topological correlations. About 10 $t\bar{t}$ events survive ($m_t = 160$ GeV; 21 pb^{-1}) with a signal to background of about 1:10. Some further improvements may be possible through tightening cuts, using quark/gluon jet discriminators, or employing additional b -jet tagging algorithms. While it does not seem promising to use the all-jets mode as a primary discovery channel for top, it may well be useful as confirmation of signals seen in other channels.

7. Conclusions

Although no breakthrough discoveries were reported in this Workshop, an enormous body of new data was presented which broadly advances our understanding of fundamental processes. Significant improvements were reported in our knowledge of the W mass and on the limits for the top quark. Studies of the strong interaction were extended to new kinematic regimes and have achieved new levels of precision. The ability of the hadron collider experiments to make incisive measurements of b -quark hadrons has been clearly demonstrated. Great credit goes to the excellent work by many individuals in the experimental and theoretical communities. Particular appreciation is due to Prof. K. Kondo and his colleagues at Tsukuba University for their organization of a congenial and productive workshop.

During this meeting, the cancellation of the SSC was announced. We are profoundly disappointed by this diminishment of our future potential. However, we have learned from the wide range of new Tevatron and Sp \bar{p} S results reported here that there are still very bright prospects for fundamental discoveries about the structure of matter at small distances at hadron colliders. We look forward eagerly to the expansion of the Tevatron program in the near future, and to the continued exploration at even higher energies with future supercolliders.

REFERENCES

1. CDF Collaboration: G. Chiarelli, these proceedings.
2. UA4 Collaboration: M. Bozzo *et al.*, Phys. Lett. B147, 385 (1984).
3. E710 Collaboration: N.A. Amos *et al.*, Phys. Letters 243B, 158 (1990).
4. UA4 Collaboration: D. Bernard, *et al.*, Phys. Lett. B198, 583 (1987).
5. UA4/2 Collaboration: C. Augier *et al.*, Phys. Lett. B316, 448 (1993) and F. Djama, these proceedings.
6. CDF Collaboration: S. Miscetti, these proceedings
7. MIMI Collaboration: A. Norton, these proceedings.
8. MIMI Collaboration: C.-H. Tan, these proceedings.
9. F.M. Borzumati, B.A. Kniehl, G. Kramer, Z. Phys. C57, 595 (1993).
10. CDF Collaboration: S. Kuhlman, these proceedings.
11. S.D. Ellis, Z. Kunszt and D.E. Soper, Phys. Rev. Lett. 62, 2188 (1989); and Phys. Rev. Lett. 64, 2121 (1990); A.D. Martin, R.G. Roberts and W.J. Stirling Phys. Rev. D43, 3648 (1991).
12. DØ Collaboration: J. Kotcher, these proceedings.
13. CDF Collaboration: F. Abe *et al.*, Phys. Rev. Lett. 68, 1104 (1992).
14. DØ Collaboration: H. Weerts, these proceedings
15. CDF has previously noted the same trend: F. Abe *et al.*, Phys. Rev. Lett. 70, 713 (1993).
16. CDF Collaboration: M. Ninomiya, these proceedings.
17. S. Ellis, Z. Kunszt, D. Soper, Phys. Rev. Lett. 69, 1496 (1992)
18. V. Del Duca and C. Schmidt, DESY Preprint 93-139 (1993).
19. R.K. Ellis *et al.*, Nucl. Phys. B286, 643 (1987).
20. DØ Collaboration, F. Borcharding, these proceedings.
21. J.D. Bjorken, Phys. Rev. D47, 101 (1992).
22. J. Ohnemus, H. Baer and J. Owens, Phys. Rev. D42, 61 (1990); J. Botts *et al.*, Phys. Lett. B304, 159 (1993).
23. M. Mangano, these proceedings and references therein.
24. P. Nason, S. Dawson, R.K. Ellis, Nucl. Phys. B303, 607 (1988); Nucl. Phys. B327, 49 (1988).
25. E.L. Berger, R. Meng and W.K. Tung, Phys. Rev. D46, 1895 (1992).
26. UA1 Collaboration: C. Albajar *et al.*, Phys. Lett. B256, 121 (1991).
27. CDF Collaboration: F. Abe *et al.*, Phys. Rev. Lett. 68, 3403 (1992); Phys. Rev. Lett. 69, 3704 (1992); Phys. Rev. Lett. 71, 500 (1993).
28. DØ Collaboration: A. Maciel, these proceedings.
29. CDF Collaboration: D. Crane, these proceedings.
30. UA1 Collaboration: A. Geiser, these proceedings.
31. M. Mangano, P. Nason, G. Ridolfi, Nucl. Phys. B373, 295 (1992).
32. W. Giele *et al.*, "DYRAD", Fermilab PUB 92/230 (1992).
33. DØ Collaboration: N. Graf, these proceedings.
34. DØ Collaboration: S. Igarashi, these proceedings.

35. CDF Collaboration: K. Abe *et al.* *Phys. Rev. Lett.* **71**, 1685 (1993).
36. CDF Collaboration: A. Hölscher, these proceedings.
37. Bijens and Hogeveer, *Phys. Lett.* **B283**, 434 (1992).
38. CDF Collaboration: J. Skarha, these proceedings.
39. CDF Collaboration: W. Badgett, these proceedings.
40. see K. Hikasa, these proceedings
41. DØ Collaboration: A. Spadafora, these proceedings.
42. DØ Collaboration: A. Taketani, these proceedings.
43. CDF Collaboration: K. Maeshima, these proceedings.
44. CDF Collaboration, D. Saltzberg, these proceedings.
45. DØ Collaboration, Q. Zhu, these proceedings.
46. UA2 Collaboration: J. Alitti *et al.*, *Phys. Lett.* **B276**, 354 (1992).
47. CDF Collaboration: F. Abe *et al.*, *Phys. Rev. Lett.* **65**, 2243 (1990).
48. CDF Collaboration: R. Kephart, these proceedings.
49. U. Baur, I. Hinchliffe, D. Zeppenfeld, *Int. J. Mod. Phys.*, **A2**, 1285 (1987).
50. see Y. Okada, these proceedings.
51. CDF Collaboration: C. Jessop, these proceedings
52. DØ Collaboration, J.T. White, these proceedings.
53. CDF Collaboration, Y. Kato, these proceedings.
54. H. Baer *et al.*, "ISASUSY", FSU-HEP preprint 930329 (1993) (unpublished.)
55. T. Muta, these proceedings.
56. CDF Collaboration: T. Chikamatsu, these proceedings.
57. DØ Collaboration: M. Fatyga, these proceedings.
58. R.H. Dalitz and G.R. Goldstein, *Phys. Lett.* **B287**, 225 (1992); K. Kondo, T. Chikamatsu and S. Kim, *Journal of the Phys. Soc. of Japan*, **62**, 1177 (1993).
59. DØ Collaboration: H. Greenlee, these proceedings.
60. CDF Collaboration: M. Contreras, these proceedings.
61. R.K. Ellis, *Phys. Lett.* **B259**, 492 (1991).
62. E. Laenen, Fermilab PUB-93/155-T (1993) (unpublished).
63. CDF Collaboration: P. Tipton, Proceedings of the 16th International Symposium on Lepton Photon Interactions (Ithaca NY) Aug. 1993.
64. CDF Collaboration: B. Denby, these proceedings.